Submitted June 2007

Detection and Classification of Weld Discontinuities in Radiographic Images (Part III: Unsupervised Learning — Phenomenological Analysis)

by Germano X. de Pádua,* Romeu R. da Silva,† Domingo Mery,‡ João M.A. Rebello§ and Luiz P. Calôba**

ABSTRACT

This is the third and final installment of a three-part article on detection and classification of discontinuities appearing in radiographic images of welds. The present installment is the continuation of the section on unsupervised pattern recognition. In this work, the authors present the phenomenological analysis of the pattern profiles of weld discontinuities that resulted from the adaptive resonance theory (ART) networks that were carried out. It is recommended that the previous parts of this article (de Pádua et al., 2007a; 2007b) be read before the present installment.

Keywords: *transversal gray level profiles, adaptive resonance theory, weld discontinuities, radiography, nondestructive testing.*

RESULTS

Phenomenological Analysis of the Patterns Generated

Phenomenological analyses of the patterns were made individually for each class from the situations considered to be the best relations between D and N in the graphs presented in Figure 5 of Part II of this article (de Pádua et al., 2007). This is in agreement with the literature (Duda et al., 2001), and was followed by visual analyses of the patterns obtained individually (Figures 6 through 10 in Part II). These analyses are as follows.

- No discontinuity class: from the $D \times N$ graph, the optimum point, which is the point where this curve undergoes an inflection, would be given by three patterns (Figure 5a in Part II). However, from visually analyzing these three patterns (Figure 6a in Part II), it is seen that there is a significant similarity between two of them (the blue and black lines), and they can be represented by only one pattern; the two resulting patterns, generated from a larger vigilance parameter, are presented here in Figure 1.
- Porosity class: in the $N \times D$ graph (Figure 5b in Part II), two points are seen that are interesting to analyze (point 2 and around point 10). The patterns generated are considered nonsimilar; however, the similarity between some of the nine patterns seems reasonable in their individual analysis (Figure 7b in Part II), therefore, we adopted two patterns to represent this class. These patterns are represented in Figure 2.
- Longitudinal crack class: in the $N \times D$ graph, the point of change of the slope is seen in four patterns (Figure 5c in Part II), but when

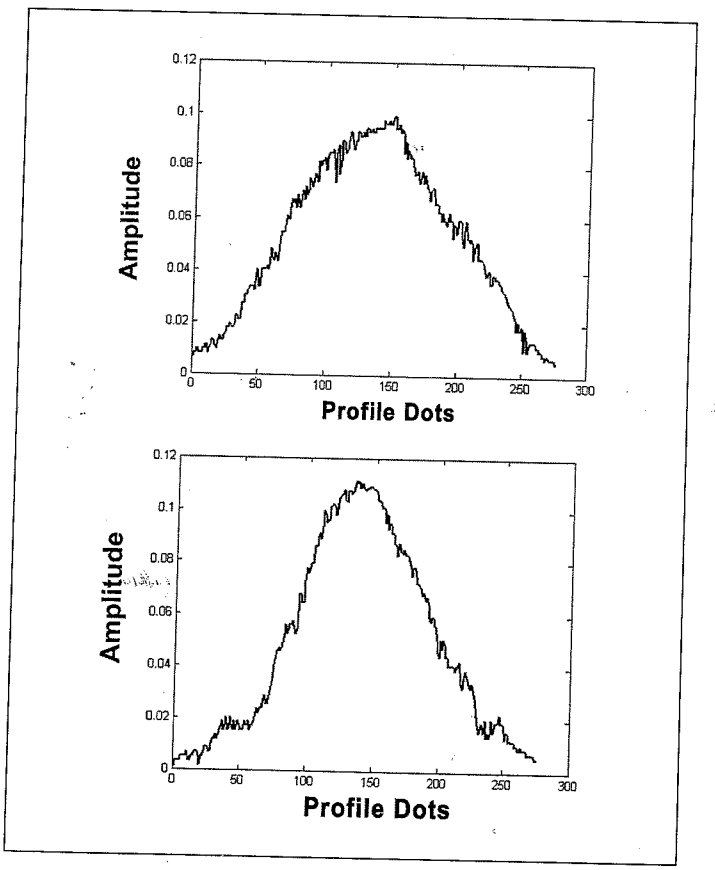

Figure 1 — The two patterns that represent the no discontinuity class.

* Petróleo Brasileiro SA – Petrobras, 81 Alm. Barroso Av. 27th floor, Rio de Janeiro, RJ, Brazil, e-mail <germanox@petrobras.com.br>.
† Departamento de Ciencia de la Computación, Pontificia Universidad Católica de Chile, Av. Vicuna Mackenna 4860(143), Santiago, Chile; e-mail <romeu@romeu.eng.br>.
‡ Departamento de Ciencia de la Computación, Pontificia Universidad Católica de Chile, Av. Vicuna Mackenna 4860(143), Santiago, Chile; e-mail <dmery@ing.puc.cl>.
§ Department of Metallurgical and Materials Engineering, Federal University of Rio de Janeiro (UFRJ), PO Box 68505, CEP 21945-970, Rio de Janeiro, RJ, Brazil.
** Department of Electrical Engineering, Federal University of Rio de Janeiro (UFRJ), PO Box 68504, CEP 21945-970, Rio de Janeiro, RJ, Brazil.

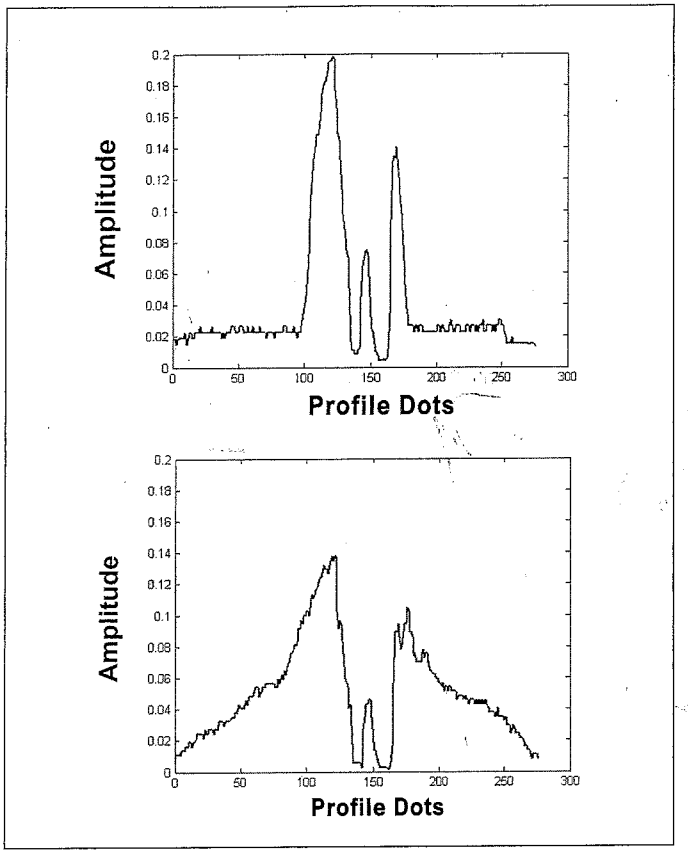

Figure 2 — The two patterns that represent the porosity class.

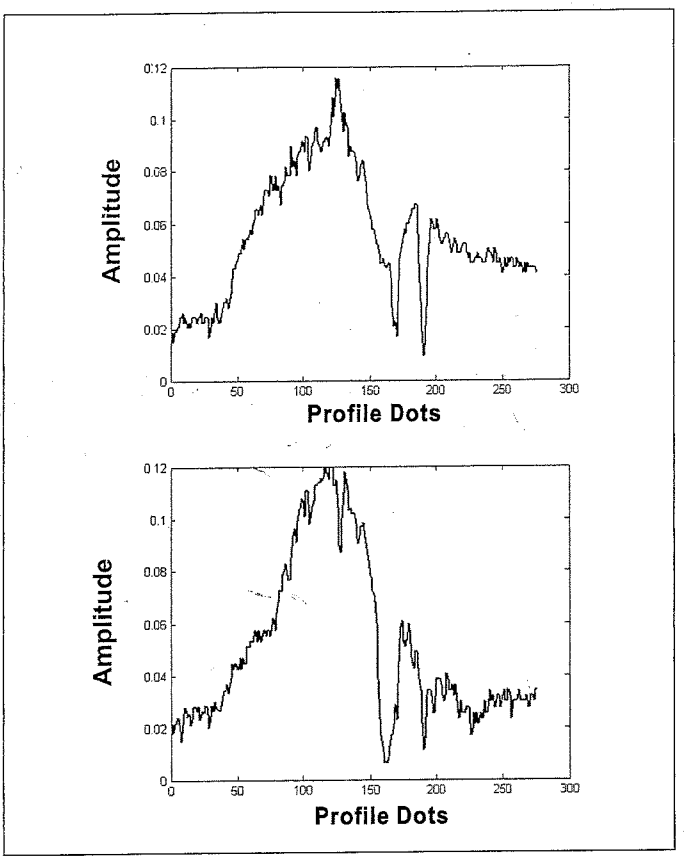

Figure 4 — The two patterns that represent the slag inclusion class.

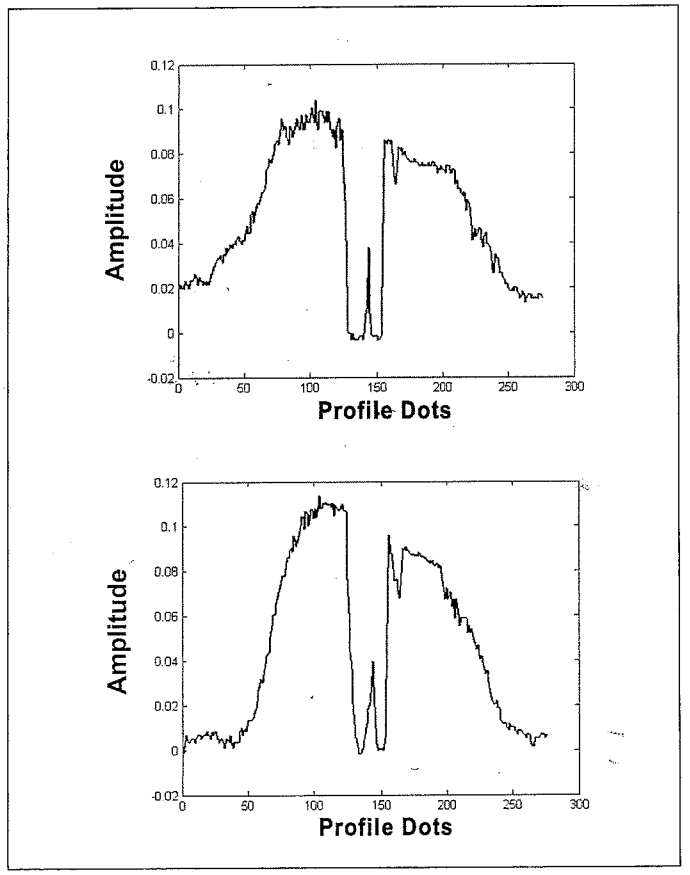

Figure 3 — The two patterns that represent the longitudinal crack class.

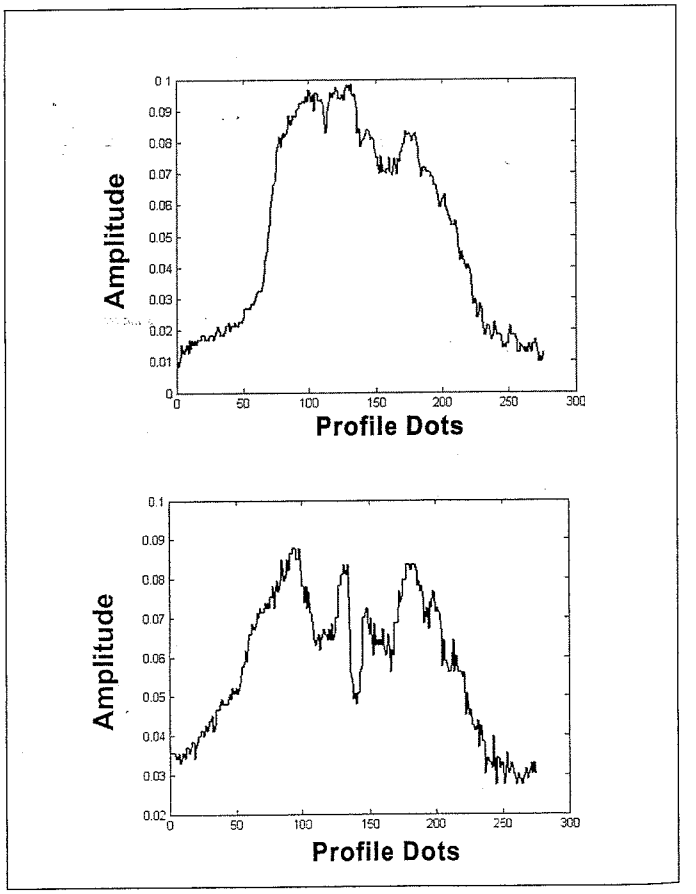

Figure 5 — The two patterns that represent the lack of fusion class.

these patterns are analyzed visually, considerable similarity is seen between them (Figure 8a in Part II). To reduce the number, the situations with 1, 2 and 3 patterns were analyzed, yet considerable similarity was still identified. Finally, a situation with two patterns was adopted, as shown here in Figure 3.

- Slag inclusion class: the $N \times D$ graph has two points of interest, localized in two and five patterns (Figure 5d in Part II). The visual analysis of these patterns (Figures 9a and 9b in Part II) indicates that with two patterns a good representation is obtained. The two patterns adopted are reproduced separately in Figure 4.
- Lack of fusion class: when analyzing the $N \times D$ graph of this class, two possible inflection points are seen in two and four patterns (Figure 5e in Part II). When visualizing these patterns, it is found that some of them are similar and can be compressed with some reservations. The two patterns shown in Figure 10a of Part II were adopted as "natural," and are shown separately in Figure 5.
- Lack of penetration class: the $N \times D$ graph of this class is quite didactic, showing two points (2 and 7 patterns) where an analysis is necessary (Figure 5f in Part II). When there are two patterns, they are quite characteristic and important from the standpoint of being representational of this class; in the visualization with seven patterns, great similarity is seen between some of them (Figure 11b in Part II). Therefore, two patterns were adopted to represent this class, and they are presented separately in Figure 6.
- Class undercut: in the $N \times D$ graph (Figure 5g in Part II), it is clearly seen that the sharpest changing point of the slope is found with three patterns. However, visual analysis of these patterns shows considerable similarity between two of them (Figure 12b in Part II), leaving only two patterns that are shown separately in Figure 7.

The Modified Adaptive Resonance Theory Network as Classifier

In addition to the primary objective of obtaining the patterns, the network was tested as a classifier with the pattern situations defined above. The result obtained, however, was much lower than with the supervised network of the backpropagation type (as discussed in Part I). This is because in order to obtain a low number of "natural" patterns, the vigilance parameter must be small, leading to a very large radius of similarity (in our case around one) and consequently a great class invasion. To use the network as a classifier, an optimized radius must be used to define the domains, as described in Part II. Examining the intraclass distances — that is, between the inputs of the same classes of discontinuities (d_{ij}) — we get the histograms shown in Figure 8.

It is seen that the distribution of the distances between the samples of each class is approximately normal, concentrating practically within the same zone for all the classes, and that was advantageous for this study. This survey allows the evaluation of the performance of the populations of each class and the estimation of the value of their radius of similarity when giving a definition of the patterns of classes and subclasses. From the histograms, a small, conservative value was adopted for the smallest mode, m, of each distribution, and from it and the criterion defined in Part II, the vigilance parameter ρ of each class was defined, where:

$$\rho = 1 - \frac{(1.5m)^2}{2} \quad (1)$$

The use of smaller similarity radii should lead to a quite greater number of patterns and better discrimination of class domains, allowing the use of the network also as a classifier. The vigilance parameters were established from the lowest mode of each class. For the lack of fusion class, $\rho = 0.989$ was the largest of them. For the no discontinuity, longitudinal crack, lack of penetration and undercut classes, $\rho = 0.955$ was established; for the slag inclusion class, $\rho = 0.975$, and for the porosity class, $\rho = 0.899$.

Considering that the similarity radii are not much different from each other, it is concluded that it would be better to use the same radius for all the classes due to the great ease of implementation that it would bring. Since the radius found for each class is the maximum

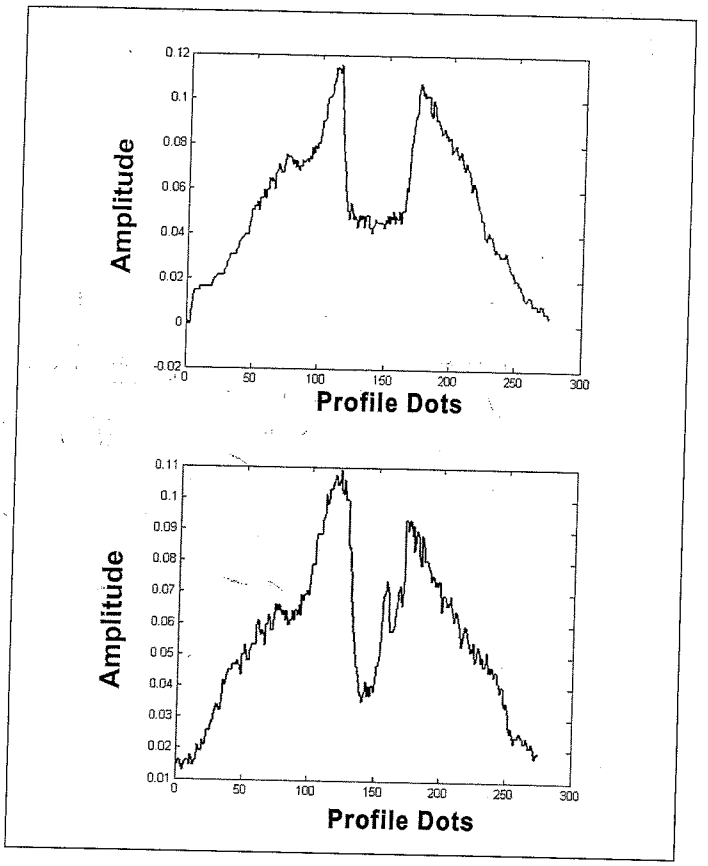

Figure 6 — The two patterns that represent the lack of penetration class.

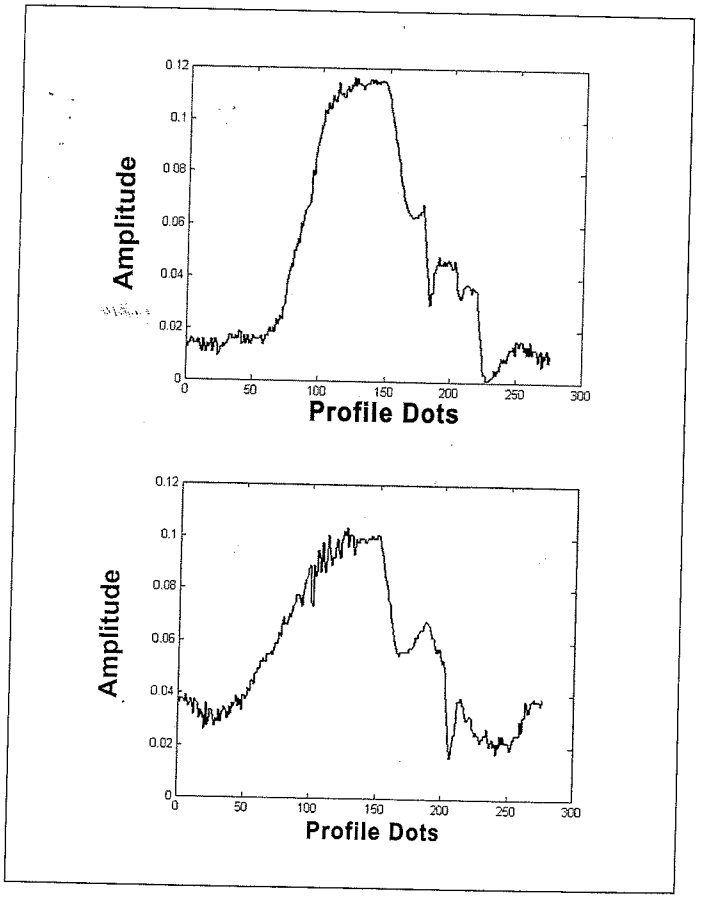

Figure 7 — The two patterns that represent the undercut class.

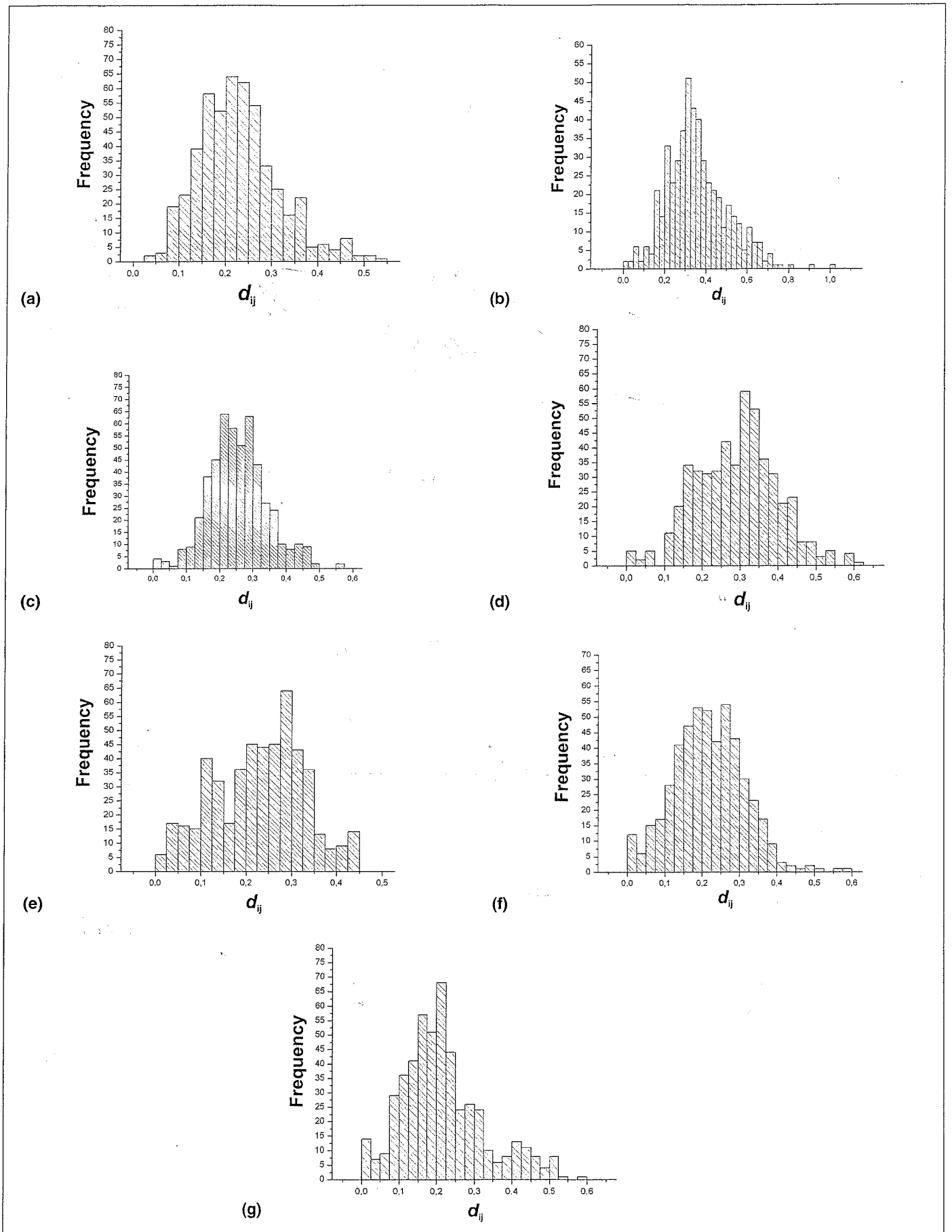

Figure 8 — Distribution histograms of the distances between the samples: (a) for the no discontinuity class, m = 0.2 (mode); (b) for the porosity class, m = 0.30 (mode); (c) for the longitudinal crack class, m = 0.20; (d) for the slag inclusion class, m = 0.15; (e) for the lack of fusion class, m = 0.10; (f) for the lack of penetration class, m = 0.20; (g) for the undercut class, m = 0.20.

suggested value, we used the smallest of them, $r = 0.15$, which corresponds to $m = 0.10$, found for the lack of fusion class, and that gives a vigilance parameter $\rho = 0.989$. Applying the procedure, the number of patterns for each class presented in Table 1 was obtained.

Table 1 Number of patterns per class (with $\rho = 0.989$ for all the classes)

Class	Number of Patterns
No discontinuity	26
Porosity	55
Longitudinal crack	22
Slag inclusion	31
Lack of fusion	7
Lack of penetration	16
Undercut	12

The greater number of patterns in the classes that would admit larger radii is an indication that the use of larger radii in these classes is possible in principle.

Tables 2 and 3 show the results obtained from confusion between the classes for the training and testing sets.

The answer "no class" indicates that no neuron was activated for a given input. The errors shown in the confusion tables are "invasions" that can be corrected by the reduction of the radius of similarity of the neuron that suffered the invasion and was activated mistakenly, but in principle this procedure requires retraining the network specialized in the class, to fill with other neurons possible voids left by the radius reduction. To test this hypothesis, an even smaller radius of similarity was used, $r = 0.10$, which is less susceptible to being invaded; this new radius led to a considerably greater success rate than that of the table, but at the expense of a substantial increase in the number of patterns, which was expected and undesirable. Considering the current success rates (Tables 3 and 4), although smaller than those obtained with the supervised trained network with backpropagation (Part I), it is important to stress once again that the main objective of this work was to find patterns representative of transverse profiles of gray levels for each typical weld discontinuity, and it can be considered an original work.

CONCLUSION

With the increasing amount of research being conducted on developing an artificial intelligence system for the analysis of radiographic images — mainly of welds (de Pádua et al., 2007a; 2007b), as is the case of this work — it is very important that the research be directed toward the various possible work "roads." The main objective of this work was to contribute new results in relation to the use of transverse profiles of gray levels for the detection and classification of discontinuities, normally used in place of the geometric and textural characteristics of the discontinuities.

It was found that it is possible to obtain patterns representative of profiles for each class of discontinuity or for a class without discontinuities. The results were satisfactory and can be used together with image processing techniques that generally make up the first part of the development of the intelligent system. It is possible that discontinuity profile patterns could be used in doubtful situations of visual classification of welding discontinuities, comparing a transverse profile with a discontinuity visualized with a pattern obtained by semisupervised training.

As to the classification indices, they were significantly lower than those achieved with the supervised training by backpropagation of error, dealt with in Part I; that was expected, because supervised training usually gives fewer classification errors. Keeping in mind that these were initial tests and we can improve the processes of profile optimization and further variations of the similarity radius, it can be considered that these tests were satisfactory, mainly for classes like longitudinal cracks and porosity, which had success rates close to 90%.

ACKNOWLEDGMENTS

The authors wish to acknowledge the National Council for Scientific and Technological Development, CAPES (Higher Level Training Agency), FAPERJ (Research Foundation of Rio de Janeiro) and the International Institute of Welding and Bundesanstalt für Materialforschung und -prüfung (Berlin) for permission to publish the radiographic patterns used in the present work.

This work has been partially supported by a grant from the School of Engineering at Pontificia Universidad Católica de Chile.

REFERENCES

de Pádua, Germano X., Romeu R. da Silva, Domingo Mery, Marcio H.S. Siqueira, João M.A. Rebello and Luiz P. Calôba, "Detection and Classification of Weld Discontinuities in Radiographic Images (Part I: Supervised Learning)," *M.E.*, Vol. 65, No. 11, November 2007a, pp. 1139–1145.

de Pádua, Germano X., Romeu R. da Silva, Domingo Mery, João M.A. Rebello and Luiz P. Calôba, "Detection and Classification of Weld Discontinuities in Radiographic Images (Part II: Unsupervised Learning)," *Materials Evaluation*, Vol. 65, No. 12, December 2007b, pp. 1230–1237.

Duda, R.O., P.E. Hart and D.G. Stork, *Pattern Classification*, second edition, Hoboken, New Jersey, Wiley, 2001.

Table 2 Confusion table for the training set

Class	Confusion(%)							
	No Discontinuity	Porosity	Longitudinal Crack	Slag Inclusion	Lack of Fusion	Lack of Penetration	Undercut	None
No discontinuity	71	8	4	5	1	9	2	0
Porosity	3	94	1	0	0	2	0	0
Longitudinal crack	2	4	91	1	1	1	0	0
Slag inclusion	4	1	3	89	2	1	0	0
Lack of fusion	8	4	0	0	88	0	0	0
Lack of penetration	12	1	1	1	0	85	0	0
Undercut	1	0	0	0	0	0	99	0

Table 3 Confusion table for the testing set

Class	Confusion (%)							
	No Discontinuity	Porosity	Longitudinal Crack	Slag Inclusion	Lack of Fusion	Lack of Penetration	Undercut	None
No discontinuity	66	9	6	2	0	13	3	1
Porosity	4	87	0	1	0	5	0	4
Longitudinal crack	2	2	92	2	0	2	0	0
Slag inclusion	10	7	0	80	0	0	0	3
Lack of fusion	0	25	0	0	58	17	0	0
Lack of penetration	19	3	6	0	0	72	0	0
Undercut	11	0	0	0	0	5	84	0